Dynamic Range and Switching Speed Limitations of an $N \times N$ Optical Packet Switch Based on Low-Gain Semiconductor Optical Amplifiers

Chien Tai and Winston I. Way, *Senior Member, IEEE*

Abstract*— Two important system performance limitations—dynamic range and switching speed—of an integrated packet switch fabric based on low-gain semiconductor optical amplifiers (SOA's) have been examined by using cascaded blocks of an SOA model, which includes transient effect, nonlinear pulse distortion effect, and amplified spontaneous emission (ASE) noise. Low-gain SOA's were used to minimize ASE noise considering that no optical filters can be integrated in an SOA-based switch fabric. The system performance with and without a narrowband optical filter at the receiver were both studied. By assuming fixed-wavelength transmitters and no optical filter can be used at the receiving end owing to the unpredictability of arriving packet wavelengths, our simulation results indicate that the dynamic ranges of 4×4 and 8×8 SOA-based packet switches at 2.5 Gb/s can only be about 3.2 and 0.8 dB, respectively. However, at 155 Mb/s, even without a receiving-end optical filter, the dynamic range of each switch size can be increased by more than 17 dB as compared to the cases of 2.5 Gb/s. Note that the dynamic ranges were estimated under the conditions of a bit error rate (BER) $\leq 10^{-9}$ and a pulse distortion ratio $\leq 30\%$. We have also shown that, when an optical filter with a 1 nm bandwidth was used at the receiving end to simulate 1) a circuit-switched condition where the center wavelength of the filter can be adjusted according to the established circuit, or 2) a packet-switched condition where each receiver has a wavelength demultiplexer and a detector array, the dynamic range of 4×4 and 8×8 switches can be increased to 16.3 and 14 dB, respectively, at 2.5 Gb/s.

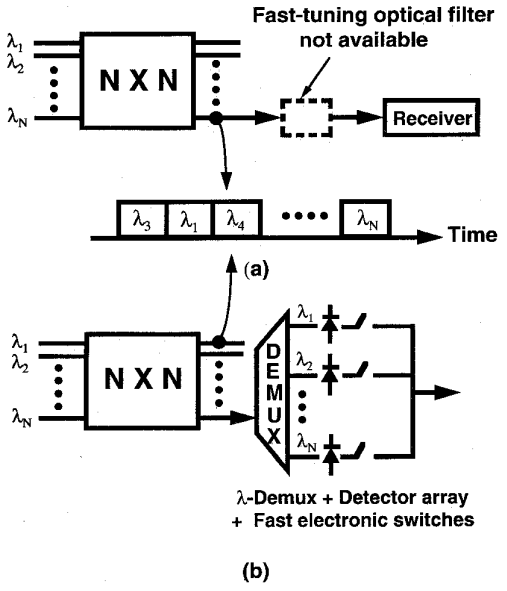

Fig. 1. In a packet-switched WDM network where transmitter wavelengths are fixed and an SOA-based switch exists, the receiver may operate without (a) or with (b) narrow-band optical filters.

I. Introduction

THE FEASIBILITY of using semiconductor optical amplifiers as switching elements in a self-routing optical packet switch has been studied extensively [1], [2]. However, considering no optical filters can be integrated in an optical packet switch, the size of an $N \times N$ packet switching fabric is severely limited owing to the amplified spontaneous emission noise-induced signal-to-noise ratio (SNR) degradation. In a WDM network, this condition may become even worse because no optical filter can be used before a photodetector owing to the unpredictability of received packet wavelengths [see Fig. 1(a)]. To alleviate this limitation, the use of low-gain optical amplifiers as switching elements has been proposed [3], [4]. However, several important system aspects such as the dynamic range and the switching speed of a low-gain-SOA-based switching fabric have not yet been investigated. Therefore, the purpose of this paper is to examine those system aspects by using cascaded SOA simulation models.

In Section II of this paper, we describe a new SOA model [5] which is based on modifying Saleh's SOA model [6]–[8]. The original Saleh's model depicted only the pattern-dependent nonlinear pulse distortion effect, whereas our modified model adds transient effect and accumulated ASE noise for completeness. Furthermore, the transient speed limitation of SOA gates is taken into account because we assume each SOA gate has a zero bias current in its OFF state to minimize the crosstalk levels in the switch. In Section III, we report detailed theoretical studies on the switching behavior and system performance of low-gain SOA-based switching fabrics. The rise and fall time of an SOA gate are investigated with respect to their dependence on the levels of injection current and input optical power. In addition, the useful dynamic range of a switching fabric which is constrained by a BER $\leq 10^{-9}$ and a cumulated pulse distortion $\leq 30\%$ is estimated for various bit-rates. The switch dynamic ranges were inves-

Manuscript received April 21, 1995; revised December 27, 1995. This work was supported by National Science Council, Taiwan, R.O.C., under Contract NSC84-2215-E009-037.

The authors are with the Department of Communication Engineering, Institute of Electro-optical Engineering, National Chiao-Tung University, Hsinchu, Taiwan, R.O.C.

Publisher Item Identifier S 0733-8724(96)02943-X.

tigated for cases with and without a receiving-end optical filter: The case without a narrow-band optical filter before the receiver is to study the condition in a WDM network where the received packet wavelengths are fast-changing and unpredictable. The case with a 1 nm optical filter is to study 1) a circuit-switched condition where the center wavelength of the filter can be adjusted according to the established circuit, or 2) a packet-switched condition where each receiver has a wavelength demultiplexer and a detector array [see Fig. 1(b)], [9]. In Section IV, we discuss the reason why the cumulative waveform distortion at 2.5 Gb/s is severe in a low-gain SOA-based packet switch. We also point out the differences in designing integrated and nonintegrated switches. Finally, the conclusions of this paper are given in Section V.

II. Nonlinear SOA Model

A. Review of Original Saleh's Nonlinear SOA Model [6]–[8]

Saleh's traveling wave SOA model is based on the following rate equation

$$\frac{dN(z,t)}{dt} = \frac{\eta I}{qV} - R[N(z,t)] - \frac{g(z,t)P(z,t)}{h\nu A} \tag{1}$$

where $N(z,t)$ is the carrier density, ηI is the current injected in the active region with a volume V and a cross-sectional area A, and η is the injection efficiency; q is the electron charge; $h\nu$ is the photon energy; $P(z,t)$ is the optical power traveling through the active region. The material gain $g(z,t)$ can be expressed as a linear function of the carrier density

$$g(z,t) \cong \Gamma a[N(z,t) - N_0] \tag{2}$$

where Γ is the confinement factor, N_0 is the carrier density at transparency, and a is the gain coefficient. $R(N)$ in (1) is the total spontaneous recombination rate which can be expressed as $R(N) = AN + BN^2 + CN^3$ where A, B, and C are the nonradiative recombination, the spontaneous emission and the Auger recombination terms [10], respectively. However, in order to get an approximate analytic solution for $N(z,t)$, a simplified expression for $R(N)$ was given by [6]

$$R(N) \approx \frac{N}{\tau_0} \tag{3}$$

where τ_0 represents a constant carrier lifetime.

Substituting (2) and (3) in (1), the dynamic rate equation became

$$\frac{dN(z,t)}{dt} \approx -\frac{[N(z,t) - N_{\rm dc}]}{\tau_0} - \frac{\Gamma a[N(z,t) - N_0]P(z,t)}{h\nu A} \tag{4}$$

where $N_{\rm dc}$ is the carrier density due to the DC bias and is given by $\eta I \tau_0/qV$. According to (2), we can express the partial derivative of N as $\partial N(z,t)/\partial t = (1/\Gamma a)\cdot \partial g(z,t)/\partial t$. By integrating (4) with respect to the entire longitudinal axis z (from 0 to L) of an SOA, we obtain the time dependent nonlinear gain equation as [6], [7]

$$\left[1 + \tau_0 \frac{d}{dt}\right][G(t) - G_0] \cong -\frac{P_{\rm out}(t) - P_{\rm in}(t)}{P_{\rm sat}} \tag{5}$$

where $G(t)$ is the total optical power gain exponent when an input signal with a power level of $P_{\rm in}(t)$ is applied to the SOA, and is given by $G(t) = \int_0^L g(z,t)dz$. The small-signal optical power gain exponent G_0 is given by $G_0 = \Gamma a(N_{\rm dc} - N_0)L$; $P_{\rm sat}$ is the amplifier saturation output power at which the power gain drops to $1/e$ of its small-signal value and is given by [8]

$$P_{\rm sat} = \frac{h\nu A}{\Gamma a \tau_0}. \tag{6}$$

It was observed that (5) can be solved approximately by using $P_{\rm out}(t) = P_{\rm in}(t)\exp(G(t))$. Depending on the degrees of accuracy and complexity, there are three kinds of approximate solutions, and they are represented by three corresponding models given in [6], [7]. The validity ranges of the above three models are for total output power levels up to about $0.1P_{\rm sat}$, $0.2P_{\rm sat}$, and $2P_{\rm sat}$, respectively [7]. Therefore, the third model which was called "large-signal model" can be used for relatively high output power. This model is shown in Fig. 2. We can see that the essence of Saleh's original model is to separate the total amplifier gain exponent into two terms, i.e., the average-power linear gain exponent $\bar{G}$, and the time-varying gain exponent $\Delta G_N(t)$ which is due to the signal induced carrier density modulation. $\bar{G}$ and $\Delta G_N(t)$ are given by [6], [7]

$$\Delta G_N(t) = F_\tau[-(P_L(t) - \overline{P_L})/P_{\rm sat}] \tag{7}$$

$$\bar{G} = G_0 + \frac{\overline{P_{\rm in}}}{P_{\rm sat}} - \frac{\overline{P_{\rm in}}}{P_{\rm sat}} e^{G_0}, \tag{8}$$

respectively. In (7), $F_\tau[\cdot]$ represents the low-pass filtering operation whose impulse response is given by $h_\tau = (1/\tau_0)\exp(-t/\tau_0)$ and τ_0 is the time constant due to the signal induced carrier density modulation; $P_L(t)$ is an intermediate power waveform that is a linearly amplified version of $P_{\rm in}(t)$ i.e., $P_L(t) = P_{\rm in}(t)\exp(\bar{G})$; and $\overline{P_L}$ is the average value of $P_L(t)$ [8]. The amplification due to $\bar{G}$ can be seen to follow the upper path in Fig. 2; and the amplification due to $\Delta G_N(t)$ follows the lower path in Fig. 2. Note that $\exp(\bar{G})$ was used to include the DC gain saturation and to extend the output power validity range of the model [7]. The amplifier output $P_{\rm out}(t)$ can therefore be expressed as $P_{\rm out}(t) = P_{\rm in}(t)e^{\bar{G}}e^{\Delta G_N(t)} = P_L(t)e^{\Delta G_N(t)}$. As illustrated in [7], [8], this model can be used to describe the pattern-dependent nonlinear distortion when an SOA was driven near or beyond their saturation output power.

B. Modification on Saleh's Large-Signal SOA Model [5]

1) Adding Transient Effects: As was mentioned earlier, the original Saleh's model depicted only pattern-dependent nonlinear pulse distortion effect. In order to consider all effects including transient behavior, nonlinear pulse distortion, and ASE noise we have modified Saleh's model, as shown in Fig. 3. Our SOA simulation block is composed of three sections. In addition to the middle section, which is Saleh's original large signal model, we have the first section to describe the transient effect, and the third section to account for the ASE noise. The SOA transient effect due to a self-routing

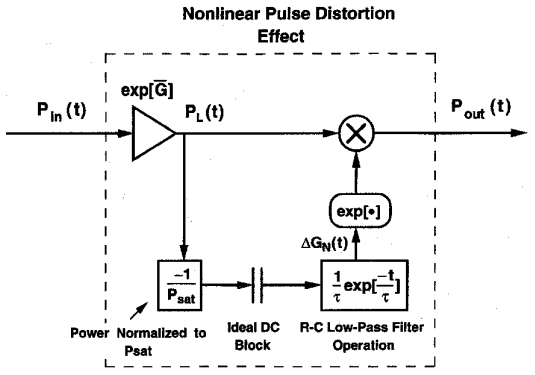

Fig. 2. Saleh's original semiconductor optical amplifier model [8].

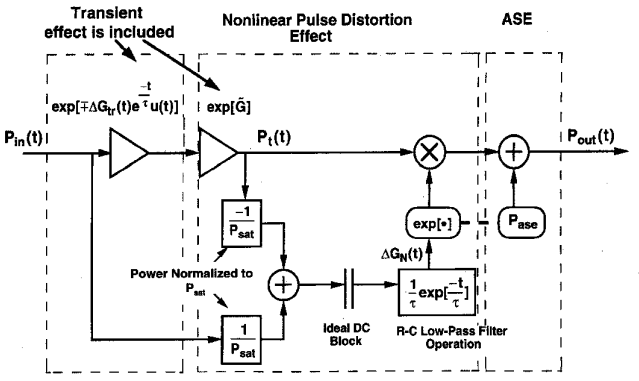

Fig. 3. The modified Saleh's semiconductor optical amplifier model by taking transient effect and ASE noise into account [5].

packet can be analyzed by applying an *electrical* current pulse to turn on or off the SOA. The corresponding rate equation is given by

$$\frac{dN(z,t)}{dt} = \frac{\eta I(t)}{qV} - R[N(z,t)] - \frac{g(z,t)P(z,t)}{h\nu A} \tag{9}$$

where $I(t)$ is the *time-varying* electrical bias. In order to find a closed-form solution for $G(t)$ which takes transient effect into consideration, we first obtain a closed-form solution for the time dependent carrier density $N(t)$ as follows. We expand $R(N)$ by a Taylor series as given by

$$R(N) \approx R(N_b) + (N - N_b)R'(N_b), \quad t' - \frac{\Delta t}{2} < t < t' + \frac{\Delta t}{2} \tag{10}$$

where Δt is an infinitesimal time interval, N_b is the instantaneous carrier density at $t = t'$ and is defined according to

$$\frac{\eta I'}{qV} = R(N_b) + \frac{g(N_b)P'(z)}{h\nu A} \tag{11}$$

where I' is the injection current at the instant $t = t'$ and $P'(z)$ is the optical power in the SOA at $t = t'$. By substituting (10) in (9), we obtain the dynamic rate equation

$$\frac{dN(z,t)}{dt} \approx \frac{\eta I(t)}{qV} - R(N_b) - (N - N_b)R'(N_b) - \frac{\Gamma a(N - N_0)P'}{h\nu A}, t' - \frac{\Delta t}{2} < t < t' + \frac{\Delta t}{2} \tag{12a}$$

if we now assume that the injection bias current is so low that it only provides the SOA a gain just enough to compensate its losses, then (12a) can be simplified to

$$\frac{dN(z,t)}{dt} = -\frac{(N - N_b)}{\tau} \tag{12b}$$

where τ is the effective carrier lifetime and is given by

$$\frac{1}{\tau} = R'(N_b) + \frac{\Gamma a P'}{h\nu A}. \tag{13}$$

Now let us assume that a step-function *electrical* current pulse $I(t)$ is applied to switch on/off the SOA, and $I(t)$ is given by

$$I(t) = I_o \pm \Delta I \cdot u(t) \tag{14}$$

for switch on $(+)$ and off $(-)$ conditions, respectively. In (14), I_o represents the injection current for the on- or off-state. Then according to (12b), we obtain a time-dependent carrier density $N'(t)$ as a function of effective carrier lifetime τ in the form of

$$N(t) = N'(t) = N_i \pm \Delta N[1 - e^{-t/\tau}]u(t), \quad t' - \frac{\Delta t}{2} < t < t' + \frac{\Delta t}{2} \tag{15}$$

where $\Delta N = N_{\text{on}} - N_{\text{off}}$; $N_i = N_{\text{on}}$ or N_{off}(N_{on} and N_{off} are the on and off steady-state carrier densities, respectively) and $N_i \pm \Delta N = N_b$. The above procedure in obtaining the time-dependent carrier density $N'(t)$ was for an arbitrary infinitesimal time interval Δt centered at t'. This procedure can be iteratively used in our computer simulation along the entire time axis and thus deduce $N'(t)$ for all t. Note that to obtain the initial condition $N'(t = 0)$, we set $\tau = \tau_0$ in (15) and $N_b = N_i$ in (13) to obtain τ_0. From (13) and (15), we can see that the SOA transient behavior depends not only on the step-size of the electrical current pulse but also on the input optical power.

After obtaining the carrier density $N'(t)$ for all t, we can use (4) with N_{dc} replaced by $N'(t)$ and τ_0 replaced by τ to obtain

$$\frac{dN(z,t)}{dt} \approx -\frac{[N(z,t) - N_0]}{\tau} \pm \frac{[\Delta N(1 - e^{-t/\tau})u(t)]}{\tau} - \frac{\Gamma a[N(z,t) - N_0]P(z,t)}{h\nu A}. \tag{16a}$$

By integrating the above rate equation with respect to the entire longitudinal axis z, we obtain the "modified" time-dependent nonlinear gain equation similar to the way Saleh derived (5)

$$\left[1 + \tau\frac{d}{dt}\right][G(t) - G_0] \cong \pm\Delta G_{\text{tr}}(t)u(t) - \frac{P_{\text{out}}(t) - P_{\text{in}}(t)}{P_{\text{sat}}} \tag{16b}$$

where $\Delta G_{\text{tr}}(t)u(t)$ is the transient gain exponent and is given by

$$\Delta G_{\text{tr}}(t)u(t) = \Gamma a L[N'(t) - N_i] \tag{17}$$

G_0 is the steady-state gain exponent for on ($G_0 = G_{\text{on}}$) or off condition ($G_0 = G_{\text{off}}$) and is given by $G_0 = \Gamma a L(N_i - N_0)$, and the instantaneous saturation output power P_{sat} is the same

as in (6) except that τ_0 is replaced by τ

$$P_{\text{sat}} = \frac{h\nu A}{\Gamma a \tau}. \tag{18}$$

The time-dependent power gain exponent can be obtained by integrating (16b) with respect to time

$$G(t) = G_0 \pm \Delta G_{\text{tr}}[1 - e^{-t/\tau}]u(t) - \int_{-\infty}^{t} \left(\frac{1}{\tau} e^{-(t-t')/\tau}\right)\left(\frac{P_{\text{out}}(t') - P_{\text{in}}(t')}{P_{\text{sat}}}\right) dt'. \tag{19a}$$

If we use (19a) and input–output relation $P_{\text{out}}(t) = P_{\text{in}}(t)\exp(G(t) - \alpha L)$ (where α is the loss coefficient of the amplifier), the two unknown variables $P_{\text{out}}(t)$ and $G(t)$ may result in an iteratively irresolvable situation. Therefore, we have to take advantage of the initial condition, i.e.,

$$P_{\text{out}}(t) = \overline{P_{\text{in}}(t)} \cdot \exp\{G_0 \pm \Delta G_{\text{tr}}[1 - e^{\frac{-t}{\tau}}]u(t) - \alpha \cdot L\} \tag{19b}$$

where $\overline{P_{\text{in}}(t)}$ represents the initial average input power. We can now decompose the solution $G(t)$ into time-varying linear gain exponents and a nonlinear gain exponent

$$G(t) \approx \mp \Delta G_{\text{tr}}(t) e^{-t/\tau} u(t) + \tilde{G} + \Delta G_N(t) \tag{19c}$$

where the first two terms represent the time-varying linear gain exponents and $\tilde{G}$ is given by

$$\tilde{G} \approx G_0 \pm \Delta G_{\text{tr}} u(t) - \alpha \cdot L + \left[\frac{\overline{P_{\text{in}}(t)} - \overline{\left(P_{\text{in}}(t) e^{\mp \Delta G_{\text{tr}} u(t) e^{-t/\tau}}\right) e^{G_0 \pm \Delta G_{\text{tr}} u(t) - \alpha \cdot L}}}{P_{\text{sat}}}\right]. \tag{20}$$

It should be noted that the effect of the step function-like electrical bias is clearly included. The last term $\Delta G_N(t)$ in (19c) represents the nonlinear gain exponent and is given by

$$\Delta G_N(t) = \left[\frac{1}{\tau}\exp(-t/\tau)\right] \otimes \left[-\frac{P_t(t) - \overline{P_t(t)}}{P_{\text{sat}}} + \frac{P_{\text{in}}(t) - \overline{P_{\text{in}}(t)}}{P_{\text{sat}}}\right] \tag{21}$$

where $\otimes$ represents a convolution operation. $P_t(t)$ is an intermediate power waveform that is an amplified version of $P_{\text{in}}(t)$ (see Fig. 3) and is expressed as

$$P_t(t) = P_{\text{in}}(t)\exp(\mp \Delta G_{\text{tr}}(t) e^{-t/\tau} u(t) + \tilde{G}) \tag{22}$$

where the signs "−" and "+" represent the switch on and off conditions, respectively. It should be noted that $\Delta G_{\text{tr}}(t)$ in (17) approaches zero under steady state condition when a constant injection current is applied. Therefore, we can see that the components $\mp \Delta G_{\text{tr}}(t) e^{-t/\tau} u(t) + \tilde{G}$ in (19c) reduces to the DC gain component $\tilde{G}$ given in (8) if αL is neglected.

2) Adding Amplified Spontaneous Emission (ASE) Noise: In addition to the total nonlinear gain exponent, ASE noise power P_{ase} was also added at the output of the SOA as shown in the third section of Fig. 3

$$P_{\text{ase}}(t) = 2n_{\text{sp}}[e^{G(t)} - 1]h\nu\Delta f \tag{23}$$

where $2n_{\text{sp}}$ represents optical amplifier noise figure, Δf is the amplifier optical bandwidth. Noted that ASE noise is neglected during transient time because ASE noise is negligible for an SOA operating at an absorption state.

Once $\tilde{G}, \Delta G_{\text{tr}}(t), \Delta G_N(t)$, and P_{ase} are all known, the modified Saleh's large-signal nonlinear amplifier model which considers transient effect, nonlinear pulse distortion, and ASE noise can be readily derived as shown in Fig. 3. The output optical power from this model can simply be expressed as

$$P_{\text{out}}(t) = P_{\text{in}}(t)\exp[\mp \Delta G_{\text{tr}}(t) e^{-t/\tau} u(t) + \tilde{G} + \Delta G_N(t)] + P_{\text{ase}}(t). \tag{24}$$

III. System Considerations of a SOA-Based Packet Switch

In this section, we will use the SOA model developed in Section II-B to estimate two important system parameters of a low-gain-SOA based packet switching fabric.

The first parameter is the switching speed limitation of each SOA gate and the second parameter is the dynamic range of the entire switching fabric. It should be noted that we have chosen a 0 mA bias current for the off-state of the SOA gates. The combination of low-gain and 0 mA off-state can offer the following advantages: 1) the high absorption at the 0 mA off-state can minimize the crosstalks in the switching fabric, 2) the accumulated ASE noise can be minimized, and 3) relatively high SOA facet reflectivities can be tolerated for low-gain SOA's [2], [11]–[13] which make fabrication processes easier.

The second parameter is the input optical power dynamic range. This parameter is bounded by the maximum input signal power (which is limited by the nonlinearity-induced pulse distortion) and the minimum input signal power (which is required to obtain a BER of 10^{-9}).

A. Switching Speed Limitation

In order to study the switching speed limitation of an SOA, we let the SOA's be switched on/off by a step-function electrical current pulse. We assumed the SOA switching speed is only affected by its carrier lifetime, and not by the electrode circuit parasitics. Also, we neglect the ASE noise term in the transient analysis. If we define τ_R as the rise time which is required for P_{out} to change from 10 to 90% of its total on/off value, and use the parameter values given in Table I, we can obtain τ_R as a function of P_{in} by using our computer simulation model. In Fig. 4, our simulation results are compared with those of a previously published numerical method [2]. We found that the discrepancy between the two results is as small as 10% under $P_{\text{in}} < -20$ dBm, is about 30% when $P_{\text{in}} > -10$ dBm. This discrepancy is because that we have linearized the total recombination rate $R(N)$ and the material gain $g(N)$, while [2] has included higher order terms

TABLE I
1.3 μm SOA PARAMETERS USED IN OUR CALCULATIONS [2], [20]

	Parameter	Value
Γ	Confinement factor	0.3
a	Gain coefficient	8.15×10^{-16} cm^2
A	Cross-section area	2.6×10^{-9} cm^2
L	Amplifier length	310 μm
$2n_{sp}$	Noise Figure	6 dB
α	Loss coefficient	20 cm^{-1}
N_0	Transparency density	1.503×10^{18} cm^{-3}
V	Active volume	8.1×10^{-11} cm^3
$R(N)=AN+BN^2+CN^3$	Recombination rate	A = 0.2 ns^{-1} $B = 1.5\times10^{-19}$ cm^3 · ns^{-1} $C = 9\times10^{-38}$ cm^6 · ns^{-1}

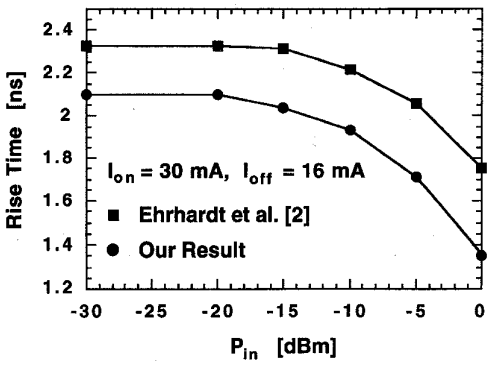

Fig. 4. Results of the obtained rise-time τ_R as a function of the input optical power P_{in} according to our block-oriented simulation model and a previously published numerical method [2].

for both parameters. Because of the longer carrier life time under small-signal condition, the switching speed limitation can be readily determined under that condition. Hence a 10% discrepancy is acceptable. Fig. 5 depicts the output power as a function of time when the SOA pump current is a step-function current pulse with $I_{\text{off}} = 0$ mA or 16 mA and $I_{\text{on}} = 34$ mA for $P_{\text{in}} = -20$ dBm. When $I_{\text{on}} = 34$ mA, we can see that the turn-on delay plus the pulse rise time at $I_{\text{off}} = 0$ mA is about 3.4 ns. This is slightly longer than the 2.8 ns at $I_{\text{off}} = 16$ mA, and is due to the strong absorption effect of SOA at a completely off-state. Fig. 5 also shows that rise time is generally longer than fall time; this is because the short carrier lifetime (high carrier density) at the beginning of the switch-off operation [2], [14]. In addition, Fig. 6 shows the turn-on delay plus rise-time as a function of the optical input power for two different values of off-state bias currents, i.e., $I_{\text{off}} = 0$ or 16 mA ($I_{\text{on}} = 34$ mA). We can see that the turn-on delay plus rise time is slightly longer for $I_{\text{off}} = 0$ mA and decreases with increasing optical input power owning to the gain saturation at higher input optical power.

B. Analysis of Cascaded SOA Gates

As a first step for estimating dynamic range, we calculate the SNR after a chain of cascaded SOA's. In order to estimate how many stages of SOA are needed in certain switch architecture, we choose dilated Benes architecture as an example. The basic

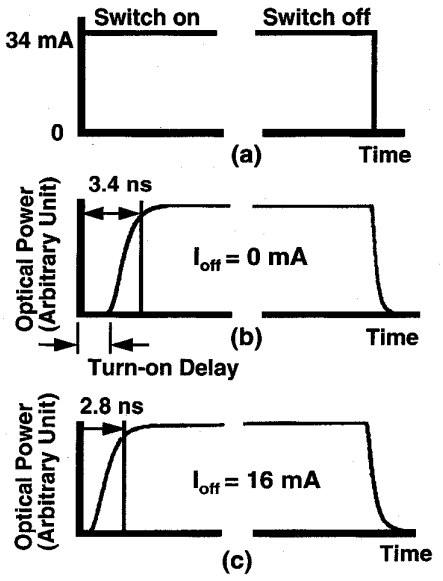

Fig. 5. (a) Electrical bias currents to turn on/off the SOA, and the corresponding transient on/off characteristics of the amplified optical pulses for (b) $I_{\text{off}} = 0$ mA and (c) $I_{\text{off}} = 16$ mA. Note that $P_{\text{in}} = -20$ dBm for both cases.

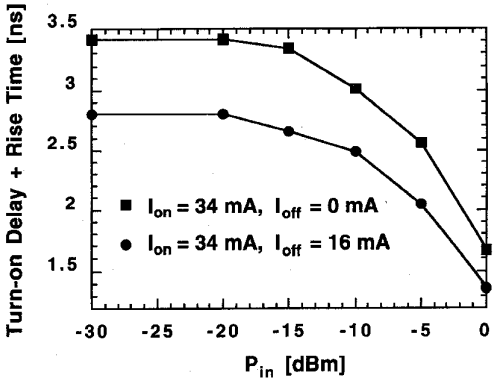

Fig. 6. Simulation results for the turn-on delay plus rise time versus the optical input power for $I_{\text{on}} = 34$ mA and two different levels of I_{off}, i.e., 0 and 16 mA.

configuration of a 2×2 switching element is illustrated in Fig. 7. It consists of an integrated 2×3 waveguide coupler, two low-gain SOA's, and a header processor. The architecture was chosen because 1) the dilated feature ensures minimization of crosstalk levels [4], 2) it uses a minimum number of optical amplifiers and a small number of couplers, 3) it has very good modularity and scalability, and 4) it is rearrangeable nonblocking [4], [15]. The small-signal internal gain of each SOA is adjusted to compensate the total loss in such a way that the net gain of the $N \times N$ switch is 0 dB. It is noted that in our calculation the 2×3 coupler loss, the 2×2 coupler loss, the fiber-waveguide (or waveguide-fiber) coupling loss, and the SOA material loss are assumed to be -5 dB, -3 dB, -5 dB, and -2.7 dB, respectively.

SOA-based packet switching is operated as follows: after an incoming optical packet which consists of a data payload and a header enters the switch, part of its input light is split off by

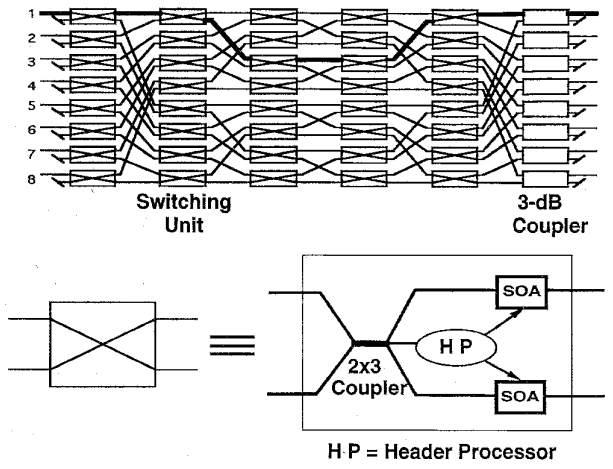

Fig. 7. An 8×8 dilated Benes switch architecture using SOA-based switching unit.

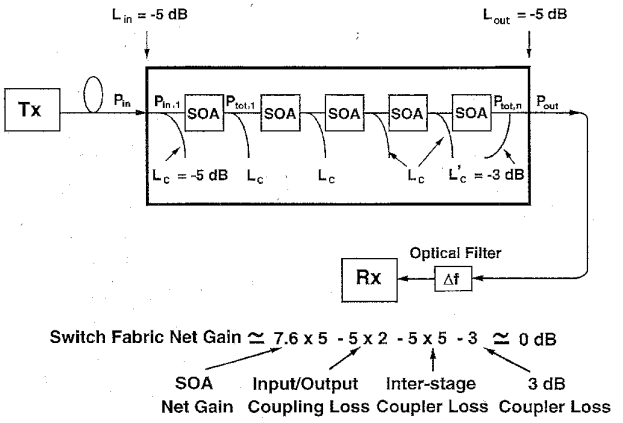

Fig. 8. Five cascaded SOA gates simulating the path traversed of an optical signal in an 8×8 SOA-based dilated Benes switch.

an optical coupler and detected by the header processor. As soon as the arriving header is captured, the header processor sends a drive current to the SOA gates and set the SOA gates in the desired configuration (on or off). Assuming no optical filters can be integrated in an SOA-based switch fabric, we have a packet traveling through the switch fabric via a route illustrated in Fig. 7. In Fig. 8, L_{in} and L_{out} represent the SOA facet coupling loss at input and output ports, respectively; L_c represents the 2×3 coupler loss, L_c' represents the loss of 2×2 directional coupler in the last stage of Fig. 7. Here we can see that an 8×8 dilated Benes switch will require 5 cascaded SOA's and the net gain of each SOA gate is about 7.6 dB so that the entire switch has a net gain close to 0 dB. Once the SOA gain is determined, the carrier lifetime τ and saturation output power P_{sat} of each SOA can be obtained accordingly, as shown in Table II (4×4 and 16×16 cases are also shown).

In Fig. 8, $P_{\text{in},1}$ is the effective input power to the first stage SOA, $P_{\text{tot},n}(n = 1, 2 \cdots i)$ is the output power of the Nth stage SOA. Considering a cascade of N identical stages, we found that $P_{\text{tot},n}(n = 1, 2, \cdots i)$ and output power (P_{out}) in

TABLE II
CARRIER LIFETIME AND SATURATION OUTPUT POWER P_{sat} USED IN OUR SIMULATION MODEL

parameters \ switch size	4x4	8x8	16x16
SOA's net gain $(10\log e^{(G_0-\alpha \cdot L)})$	9.3 dB	7.6 dB	6.8 dB
Carrier lifetime (τ)	588 ps	612 ps	623 ps
Saturation power (P_{sat})	4.41 dBm	4.25 dBm	4.17 dBm

$$G_0 = \Gamma a L (N_{dc} - N_0) \; ; \quad \tau \equiv \frac{1}{R'(N)}\bigg|_{N=N_{dc}} \text{[10]}; \quad P_{sat} = h\nu A / \Gamma a \tau \; .$$

Fig. 8 are given by

$$\begin{aligned} P_{\text{in},1} &= P_{\text{in}} \cdot L_{\text{in}} L_c \\ P_{\text{tot},1} &= P_{\text{in},1} \cdot \exp[G_1(t)] + P_{\text{ase},1} \\ P_{\text{tot},2} &= L_c \cdot P_{\text{tot},1} \cdot \exp[G_2(t)] + P_{\text{ase},2} \\ &\vdots \\ P_{\text{out}} &= L_c' L_{\text{out}} P_{\text{tot},n} \end{aligned} \tag{25}$$

where $P_{\text{ase},n}$ and $G_n(t)$ are the ASE noise and time-dependent nonlinear gain exponent of the Nth-stage SOA, and $P_{\text{ase},n} = 2n_{\text{sp}}[\exp(G_n(t)) - 1]h\nu\Delta f$, Δf is the amplifier optical bandwidth. Since we assume that no optical filter can be integrated in an SOA-based switch fabric, therefore the amplifier optical bandwidth Δf was assumed to be 40 nm for all cascaded amplifier stages. As for the optical filter before the optical receiver, two filter bandwidths were assumed: 1) $\Delta f = 40$ nm, and 2) $\Delta f = 1$ nm. Case 1) is used in a high-speed packet-swiched WDM network where a fast tuning optical filter is not available [Fig. 1(a)], and case 2) is used in a circuit-switched environment where the use of a tunable optical filter is feasible or a packet-switched environment where a wavelength demultiplexer, a detector array, and an array of fast-tuning electronic switches are available [Fig. 1(b)].

After square law detection in the receiver, the dominant electrical noise contains the signal-spontaneous beat noise (s-sp) and the spontaneous-spontaneous beat noise (sp-sp). The received noise power produced by beat terms can be expressed as [16], [17]

$$I_{\text{s-sp}}^2 = 2I_{\text{ase}} I_1 B_e / B_o \tag{26}$$

$$I_{\text{sp-sp}}^2 = I_{\text{ase}}^2 B_e / B_o \tag{27}$$

where I_1 and I_{ase} are the equivalent photocurrent of the signal power and accumulated ASE noise power, respectively. B_e is the electrical bandwidth (it is assumed to be $0.65 r_B$ where r_B is the bit rate), B_o is the optical filter bandwidth ($B_o = 40$ or 1 nm). An ideal extinction ratio from the transmitter is assumed. The BER at the receiver is given by [17]

$$\text{BER} = \frac{1}{\sqrt{2\pi}} \frac{\exp(-Q^2/2)}{Q} \tag{28}$$

where Q is given by $Q = I_1 / (\{I_{\text{noise,one}}^2)^{1/2} + (I_{\text{noise,zero}}^2)^{1/2}\}$, $I_{\text{noise,one}}^2$ and $I_{\text{noise,zero}}^2$ are the total noise powers in ONE- and ZERO-states, respectively. Equations

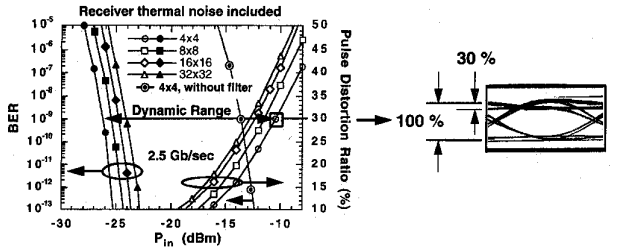

Fig. 9. BER and pulse distortion ratio versus optical input power (P_{in}) for four switch fabric sizes ($4 \times 4, 8 \times 8, 16 \times 16$, and 32×32) at 2.5 Gb/s NRZ signal. The eye diagram on the right is obtained at a distortion ratio of 30%.

(25)–(28) form the basis from which the BER performance of the SOA-based switching system is evaluated.

By assuming a receiver thermal noise level which gives a receiver sensitivity of -28 dBm at 2.5 Gb/s, we obtained in Fig. 9 the results of NRZ BER and pulse distortion ratio as a function of average input optical power. The BER penalty was due to the accumulated ASE noise in the switch fabric, and the pulse distortion ratio was due to the large input optical power induced nonlinear gain saturation. By defining the dynamic range of an optical packet switch as the input optical power range which is constrained by a specified BER ($\leq 10^{-9}$) and a specified pulse distortion ratio ($\leq$30%), we can see that the dynamic range of a 4×4 switch is only 3.2 dB when no receiver optical filter is used, and is significantly improved to 16.3 dB when an optical filter with a passband of 1 nm is used. In this case, even a 32×32 switch can maintain a dynamic range of 11 dB.

Fig. 10 summarizes the results on dynamic range as a function of switch size for 2.5 Gb/s and 155 Mb/s, respectively. Solid curves are obtained from Fig. 9, with and without receiving-end optical filter, at 2.5 Gb/s. Dashed curves are for 155 Mb/s and for cases with and without receiving-end optical filters, respectively. Thermal noise was neglected at this low bit rate. From Fig. 10, we can see that at 155 Mb/s, with or without receiving-end optical filter, the dynamic ranges of a 256×256 switch are about 15 dB and 32 dB, respectively. Note that we have assumed $P_{\text{in}} < 0$ dBm and no pulse distortion was observed even at this high level of P_{in}. This result suggests that, at 155 Mb/s the SOA-based photonic switch can be used without any optical filters and still achieve an appreciable dynamic range.

IV. Discussion

From the above simulation results, we know that when SOA's are driven near saturation due to cascaded SOA's generate cumulative spontaneous emission noise, their inherent nonlinearity causes significant bit-pattern-dependent pulse distortion, particularly in the multigigabit range. The degree of nonlinear pulse distortions can be estimated from a so called "normalized bit-rate parameter" which was defined as the product of the bit rate and the amplifier's carrier lifetime $r_B \cdot \tau$ [8]. A significant intersymbol interference (ISI) penalty could be incurred if $r_B \cdot \tau \approx 1$, because the population inversion changes cannot reach a steady state during the bit duration ($1/r_B$). Under this condition, the "memory"

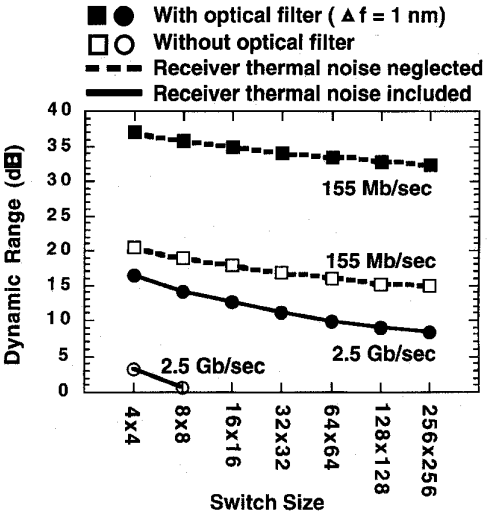

Fig. 10. Dynamic range versus switch fabric size for 155 Mb/s and 2.5 Gb/s NRZ signals. Both cases with and without optical filters are shown. The 2.5 Gb/s receiver has a thermal noise-limited receiver sensitivity of -28 dBm.

effect of an SOA makes the nonlinear distortion associated with a given output depend on the particular pattern of the preceding bits [8]. To illustrate this phenomenon, the upper portion of Fig. 11 shows traces of the optical waveforms at the output of an 8×8 switch at 155 Mb/s and 2.5 Gb/s, respectively, at $P_{\text{in}} = -12$ dBm. The lower portion of Fig. 11 shows the corresponding eye diagrams after a photodetector. It is obvious that the SOA pattern-dependent effect plays an important role at 2.5 Gb/s, while this pattern-dependent effect is negligible at 155 Mb/s. With this observation, it is understood that the SOA carrier lifetime must be significantly reduced so that an SOA-based switch can be operated at a multigigabit/s bit rate. However, even with a multiquantum-well optical amplifier [18], its carrier lifetime cannot be easily reduced to less than 100 ps under *low-bias* conditions. The requirement of using low-gain SOA's in an integrated packet switch (to minimize ASE noise and crosstalks in the switch) also prohibits the use of a clamped-gain SOA's which usually must be operated at high bias current [19]. It is interesting to note that, although we can decrease the SOA length instead of its bias current in order to reduce its optical gain, increased crosstalk levels in the switch may be resulted due to the decreased material absorption when the SOA is at OFF state.

The turn-on and turn-off times obtained in Section III-A were both below 3.4 ns when $I_{\text{off}} = 0$ mA and I_{on} is at a low bias level. This transient performance is acceptable considering an asynchronous transfer mode (ATM) cell with 53 bytes at 2.5 Gb/s has a duration of about 170 ns. Therefore the guard time required to turn-on and turn-off the SOA switch can be reasonably small as compared to the data packet.

It is worth emphasizing that the design considerations and system performances between *integrated and nonintegrated* SOA-based optical switches are quite different. Table III lists a set of comparisons. We can see the key difference lies in the fact that a nonintegrated SOA-based switch fabric has

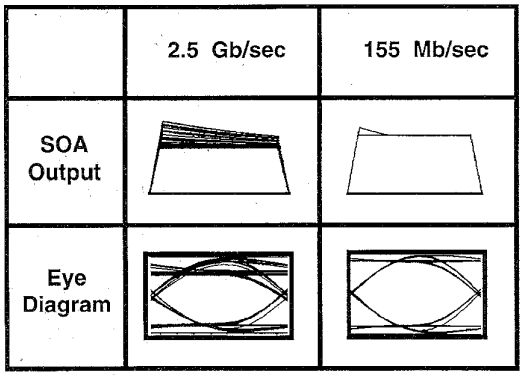

Fig. 11. Simulated optical waveforms and eye diagrams for an output signal from an 8×8 switch when $P_{\text{in}} = -12$ dBm.

TABLE III
COMPARISON OF SOA-GATE CHARACTERISTICS BETWEEN INTEGRATED AND NONINTEGRATED OPTICAL SWITCH

	Integrated	Non-integrated [2]
Interstage loss *	low (≈ -5 dB)	high (≈ -15 dB)
SOA's net gain **	low (8 ~ 10 dB)	high (16 ~ 18 dB)
Carrier lifetime	large (≥ 580 ps)	small (≤ 400 ps)
Switching speed	low (≥ 2 ns)	high (≤ 2 ns)
Pulse distortion	large	small
ASE accumulation	low	high

*Interstage loss for an SOA in a non-integrated SOA-based switch includes two facet-coupling losses (-5 dB per facet) and the 2x3 coupler loss (-5 dB).

**SOA's net gain is chosen according to a given switch fabric architecture (e.g., dilated Benes) so that the net gain of the entire switch is close to 0 dB.

less constraint on power consumptions, and therefore the bias current at ON state (I_{on}) can be much higher than that in the integrated switch. Because of this higher I_{on}, the interstage loss can be higher, the pulse distortion is smaller (for the same input optical power), but the accumulated ASE noise is also higher.

V. CONCLUSION

In this paper, a modified SOA block-oriented model which considers nonlinear pulse distortion, transient effect, and ASE noise has been built. By using this simulation model, we examined both the switching speed limitations and dynamic range of *low-gain* SOA-based switching fabrics. The distributed low-gain operation provides advantages such as low accumulated ASE noise and easy fabrication process (because of the relatively high SOA facet reflectivities that can be tolerated). We also chose to operate these SOA gates with an OFF-state bias at 0 mA in order to minimize the crosstalks in the switch. While using these low I_{on} and zero I_{off} SOA gates, the turn-on and turn-off delays can both be below about 3.4 ns, which is only slightly longer than the corresponding delays in the case of higher I_{on} and nonzero I_{off}.

While investigating the dynamic range of an integrated SOA-based switch fabric (using a dilated-Benes architecture) which has no integrated optical filters, we found that the narrow-band optical filter at the receiver site is critical for operations at or beyond 2.5 Gb/s, even for the smallest switch size of 4×4. However, in a gigabit packet-switched network where transmitter wavelengths are fixed a fast-tuning optical filter which changes its center wavelength on a packet by packet (or cell by cell) base is practically unavailable. Therefore, a receiver with a WDM demultiplexer, a detector array, and array of fast electronic switches is necessary. In this case, the dynamic ranges of a 4×4 and 256×256 switches can reach 16.3 and 8.2 dB, respectively. On the other hand, when the network operation speed is 155 Mb/s, such as in a local area network, we found that even when no receiving-end optical filter is used, a switch dynamic range of about 15 dB can still be obtained for a switch size of 256×256. This number can be further increased to about 32 dB if a 1 nm optical filter is used.

REFERENCES

[1] R. Fortenberry, A. J. Lowery, W. L. Ha, and R. S. Tucker, "Photonic packet switch using semiconductor optical amplifier gates," *Electron. Lett.*, vol. 27, pp. 1305–1307, 1991.
[2] A. Ehrhardt, M. Eiselt, G. Großkopf, L. Kuller, R. Ludwig, W. Pieper, R. Schnabel, and H. G. Weber, "Semiconductor laser amplifier as optical switching gate," *J. Lightwave Technol.*, vol. 11, pp. 1287–1295, Aug. 1993.
[3] R. F. Kalman, L. G. Kazovsky, and J. W. Goodman, "Space division switches based on semiconductor optical amplifiers," *IEEE Photon. Technol. Lett.*, vol. 4, pp. 1048–1051, Sept. 1992.
[4] Y. K. Chen and W. I. Way, "Multiwavelength line-rate-independent optical digital cross-connects based on low-gain fiber amplifiers," *IEEE Photon. Technol. Lett.*, vol. 6, pp. 1122–1125, Sept. 1994.
[5] C. Tai and W. I. Way, "On the dynamic range and switching speed limitations of an $N \times N$ optical ATM Switch based on low-gain semiconductor optical amplifiers," in *Tech. Dig., Opt. Fiber Commun. Conf.*, San Diego, CA, 1995, paper WE3.
[6] A. A. M. Saleh, "Nonlinear models of travelling-wave optical amplifiers," *Electron. Lett.*, vol. 24, pp. 835–837, 1988.
[7] ——, "Modeling of nonlinearity in semiconductor optical amplifiers," in *GLOBECOM '89 Conf. Rec.*, Dallas, TX, 1989, vol. 2, pp. 0665–0669.
[8] A. A. M. Saleh and I. M. I. Habbab, "Effects of semiconductor-optical-amplifier nonlinearity on the performance of high-speed intensity-modulation lightwave systems," *IEEE Trans. Commun.*, vol. 38, pp. 839–846, June 1990.
[9] F. Tong, C.-S. Li, A. E. Stevens, and Y. H. Kwark, "Characterization of a 16-channel optical/electronic selector for fast packet-switched WDMA networks," *IEEE Photon. Technol. Lett.*, vol. 6, pp. 971–974, Aug. 1994.
[10] R. M. Jopson and T. E. Darcie, "Semiconductor laser amplifiers in high-bit-rate and wavelength-division-multiplexed optical communication systems," in *Coherence, Amplification, and Quantum Effects in Semiconductor Lasers*, Yoshihisa Yamamoto, Ed. New York: Wiley, 1991, ch. 8.
[11] M. J. O'Mahony, "Semiconductor laser amplifies for use in future fiber systems," *J. Lightwave Technol.*, vol. 6, pp. 531–544, Apr. 1988.
[12] T. Saitoh and T. Mukai, "Recent progress in semiconductor laser amplifiers," *J. Lightwave Technol.*, vol. 6, pp. 1656–1664, 1988.
[13] J. D. Evankow, Jr., and R. A. Thompson, "Photonic switching modules designed with laser diode amplifiers," *IEEE J. Select. Areas Commun.*, vol. 6, pp. 1087–1095, Sept. 1988.
[14] L. Gillner, "Modulation properties of a near travelling-wave semiconductor laser amplifier," *IEE Proc. Pt. J*, vol. 139, no. 5, pp. 331–338, 1992.
[15] K. Padmanabhan and A. N. Netravsli, "Dilated networks for photonic switching," *IEEE Trans. Commun.*, vol. COM-35, pp. 1357–1365, Dec. 1987.
[16] C. R. Giles and E. Desurvire, "Propagation of signal and noise in concatenated Erbium-doped fiber optical amplifiers," *J. Lightwave Technol.*, vol. 9, pp. 147–154, Feb. 1991.
[17] N. A. Olsson, "Lightwave systems with optical amplifiers," *J. Lightwave Technol.*, vol. 7, pp. 1071–1082, July 1989.

[18] J. M. Wiesenfeld, A. H. Gnauck, G. Raybon, and U. Koren, "High-speed multiple-quantum-well optical power amplifier," *IEEE Photon. Technol. Lett.*, vol. 4, pp. 708–711, July 1992.
[19] G. Soulage, A. Jourdan, P. Doussiere, G. Da Loura, and M. Sotom, "Clamped-gain SOA gates as multiwavelength space switches," in *Tech. Dig., Opt. Fiber Commun. Conf.*, paper TuD1, San Diego, CA, 1995.
[20] G. Jeong and J. W. Goodman, "Gain optimization in switches based on semiconductor optical amplifiers," *J. Lightwave Technol.*, vol. 13, pp. 598–605, 1995.

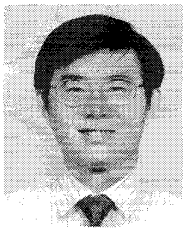

Chien Tai was born in Taiwan, Republic of China, in 1965. He received the B.S. degree in electrophysics from National Chiao Tung University, Taiwan, in 1989, and the M.S. degree in physics from National Tsing Hua University, Taiwan, in 1992. He is now pursuing the Ph.D. degree in the area of WDM photonic switching network and subcarrier multiplexed transmission systems at National Chiao Tung University, Hsinchu, Taiwan.

From 1989 to 1990, he worked as an engineer at Tyntech Corporation, Taiwan, where he was engaged in research on III-V compound semiconductor devices.

Winston I. Way (S'82–M'83–SM'88) was born in Taiwan, Republic of China, in 1955. He received the B.S. degree from the National Chiao Tung University, Taiwan in 1977, and the M.S.E.E. and Ph.D. degrees in electrical engineering and science from the University of Pennsylvania, Philadelphia in 1981 and 1983, respectively.

From 1984 to 1992, he was with Bellcore and was involved in various lightwave system research projects such as distributing satellite, digital radio, and cable television signals by using subcarrier multiplexing techniques; designing hybrid/IC regenerators for direct detection systems; designing lightwave systems that include erbium-doped fiber amplifiers, semiconductor optical amplifiers; studying system issues related to dense-wavelength-division-multiplexing and optical-frequency-division-multiplexing techniques; and studying the feasibility of applying advanced lightwave technologies to SONET/SDH self-healing rings. He is now a Professor at the Department of Communication Engineering, National Chiao Tung University, Hsinchu, Taiwan, Republic of China. His current research interests are in applying advanced lightwave techniques to public telecommunication networks, and hybrid fiber coax (HFC) networks. He has authored more than 80 journal articles and conference presentations, and holds three U.S. patents.

Dr. Way has served as a Guest Editor for IEEE JOURNAL ON SELECTED AREAS IN COMMUNICATIONS, Conference Co-chair for IEEE/LEOS Summer Topical Meeting, and has served on many IEEE LEOS and M.I.T. conference technical program committees.